LAWRENCE
LIVERMORE
NATIONAL
LABORATORY

LLNL-CONF-864496

Time resolved X-ray diffraction using the FIDDLE diagnostic at NIF: Preliminary assessment of diffraction precision

C. E. Vennari, N. E. Palmer, P. R. Nyholm, N. Bhandakar, S. R. Nagel, R. B. Petre, C. V. Stan, J. H. Eggert, D. K. Bradley, Y. Ping, A. Thomas, D. Swift, A. C. Carpenter, A. J. MacKinnon, L. R. Benedetti

May 16, 2024

25th Topical Conference on High Temperature Plasma Diagnostics
Asheville, NC, United States
April 21, 2024 through April 25, 2024

Time resolved X-ray diffraction using the Flexible Imaging Diffraction Diagnostic for Laser Experiments (FIDDLE) at the National Ignition Facility (NIF): Preliminary assessment of diffraction precision

C. E. Vennari[1,a)], N. E. Palmer[1], P. R. Nyholm[1], N. S. Bhandakar[1], S. R. Nagel[1], R. B. Petre[1], C. V. Stan[1], J. H. Eggert[1], D. K. Bradley[1], Y. Ping[1], A. Thomas[1], D. C. Swift[1], A. C. Carpenter[1], A. J. MacKinnon[1], L. R. Benedetti[1]

[1]*Lawrence Livermore National Laboratory, Livermore, California, 94550, USA*

(Presented XXXXX; received XXXXX; accepted XXXXX; published online XXXXX)

The Flexible Imaging Diffraction Diagnostic for Laser Experiments (FIDDLE) is a new diagnostic at the National Ignition Facility (NIF) designed to observe in situ solid-solid phase changes at high pressures using time resolved X-ray diffraction. FIDDLE currently incorporates five Icarus Ultrafast X-ray Imager sensors that take 2 ns snapshots and can be tuned to collect X-rays for tens of ns. The platform utilizes the laser power at NIF for both the laser drive and the generation of 10 keV X-rays for ~10 ns using a Ge backlighter foil. We aim to use FIDDLE to observe diffraction at different times during compression to probe the kinetics of phase changes. Pb undergoes two solid-solid phase transitions during ramp compression: from FCC to HCP and HCP to BCC. Results will be reported on some of the first shots using the FIDDLE diagnostic at NIF on ramp compressed Pb to a peak pressure of ~110 GPa and a single undriven CeO_2 calibration shot. A discussion of the uncertainties in the observed diffraction is included.

I. INTRODUCTION

Laser-driven dynamic compression experiments have been used extensively to investigate pressure and temperature regimes in solid and liquid materials that cannot be achieved by other means, e.g., static high pressure and temperature experiments. X-ray diffraction (XRD) is a fundamental technique used for phase (structural) identification and density measurements of both solids and liquids during dynamic compression. The goal of this new diagnostic, Flexible Imaging Diffraction Diagnostic for Laser Experiments (FIDDLE), is to gain insight into fundamental questions about the kinetics of phase transitions during dynamic compression by collecting time resolved XRD.

Light sources such as synchrotrons and X-ray Free Electron Lasers (XFELs) provide bright, coherent, and non-divergent X-ray sources, but are not coupled to laser facilities, such as the NIF, that are able to reach several Mbar with excellent pulse shaping. Other limitations to using light sources for these experiments include: no way to probe multiple times during a single shot using X-ray diffraction, repeated shots can be susceptible to variations in targets, and laser pulse shape instability between shots. There has been extensive research in generating quasi-monochromatic X-rays at the National Ignition Facility (NIF) using a subset of laser beams and a backlighter (BL) foil (*1*). By controlling the laser pulse shape, an X-ray source with length of up to 10 ns can be generated (*2*). Using two pulse shapes, one for the drive and the other for the BL X-ray source, we can time X-ray arrival on the target during dynamic compression.

The FIDDLE diagnostic incorporates five Icarus hCMOS sensors which collect XRD on the nanosecond time scale (*3*). Icarus sensors are electrically gated such that they collect up to 4 frames of data for a single shot with a dwell time between frames. The future FIDDLE diagnostic iterations will incorporate 8 Daedalus (*4*) sensors and a streak camera for continuous recording of diffraction. FIDDLE builds on techniques developed with other XRD diagnostics at NIF G3D (*5*) and TARDIS (*6*).

We report on data from both undriven and driven shots in this paper. The undriven shot, focused on diffraction from the XRD standard CeO_2 was conducted because XRD requires precise understanding of the X-ray source, sample and detector for a given experimental set up. CeO_2 is used extensively as an X-ray diffraction calibration material given its high scattering efficiency, small grain size (i.e. low texture) and relatively large number of reflections. For the driven shots, we use a physics package for linearly ramp compressed Pb. Pb has been studied extensively using static and dynamic compression and its phase diagram is well established at high pressures and temperatures (*7*). On the linear ramp compression path taken in these experiments, Pb is initially in the FCC structure and transitions to HCP then BCC. The sensors in this study are timed to observe the transition from HCP to BCC.

II. EXPERIMENT SETUP

[a)]Author to whom correspondence should be addressed: vennari1@llnl.gov

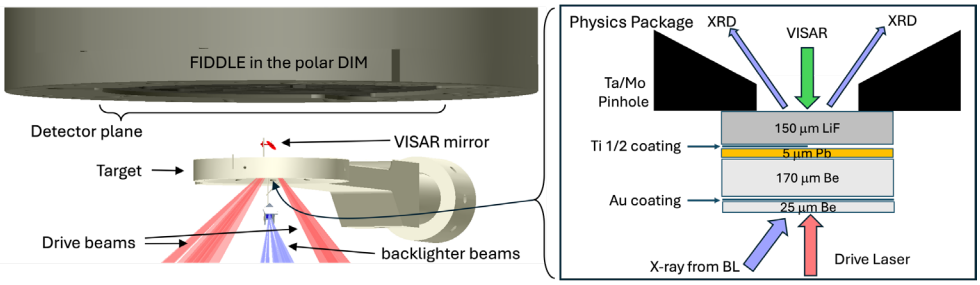

FIG. 1. (left) VISRAD representation of the experimental setup. Drive beams are represented with red; BL beams are represented with blue. (right) a depiction of the high pressure Pb physics package, not to scale.

FIDDLE is inserted above the target with the Polar Diagnostic Insertion Manipulator (Polar DIM) in the NIF target chamber (Fig. 1a). A description of the detailed FIDDLE engineering decisions and design are included in ref. (*8*). Five Icarus sensors are placed on the front surface of FIDDLE and are arranged such that they maximize the 28 and azimuthal coverage. The area not occupied by Icarus sensors is filled with a time integrated image plate. The Icarus sensors are timed in the 2-2-0 mode; in this mode, the sensors were actively collecting diffraction for 2 ns and off for 2 ns for a total of 4 active frames (over 14 ns). Sensor timing was calibrated off-line with many repetitions of a short-pulsed laser (*9*). The input triggers and timing pickoff information are multiplexed to evaluate the timing of each sensor during a shot at NIF; a detailed description of the timing can be found in ref. (*10*).

The physics package is held close to the sensors to maximize 2θ and azimuthal coverage of FIDDLE. 12 NIF beams, from 3 quads, are pointed to 3 colinear spots on a Ge BL foil to generate quasi-monochromatic 10.2 keV X-rays. The BL is surrounded by an enclosure comprised of both gold and plastic that aims to minimize the X-rays that radiate in 2ρχ. The X-rays are not collimated before the target; instead, the X-rays exit angle is controlled by a pinhole (Mo or Ta) on the downstream side of the physics package. The high-pressure targets are driven using 12 NIF beams using 3 mm continuous phase plates (CPPs) for a laterally homogeneous pressure wave. The physics package for driven targets consists of: 25 µm thick Be ablator layer / Au heat shield / 170 µm pusher layer / 5 µm Pb / ½ coating of Ti / 150 µm LiF window/tamper (Fig 1b). A mirror is mounted on the top of the target which reflects a probe laser light from the Pb/LiF interface to the Velocity Interferometer System for Any Reflector (VISAR) system on from the 90-315 port. The physics package for the undriven CeO_2 calibration target was prepared by ManTech and consisted of CeO_2 powder with a grain size of ~150 µm mixed into an Stycast 1266 epoxy resin. The resulting puck contained 1:3 CeO_2:epoxy by weight and was cut to a thickness of 20 µm, coated with 0.5 µm Au as a heat shield and mounted to a target with a Mo pinhole.

All 5 sensors were timed in the 2-2-0 mode with the first frame centered at 24.5 ns. Images from Icarus sensors were processed moderately prior to analysis: first the rod shot image was subtracted, then a 7x7 median filter was applied to the rod shot subtracted image.

III. LOCATION CALIBRATION SHOT USING CeO_2

XRD depends heavily on a knowledge of the respective locations of the X-ray source, physics package, and sensors because the observable is an angle from the incident direct beam to the observed diffraction. It is common for all high-pressure XRD instruments to have some empirical internal calibration, rather than relying on the engineered positions. This is commonly done by collecting diffraction on a known material at room pressure that diffracts well, such as, LaB_6 or CeO_2.

CeO_2 diffraction was observed on the first frame (t=24.5 ns) on 4 of the Icarus sensors (Fig. 2). Using this diffraction, we iterated on a calibration for the BL and sensor positions with the diffraction rings shown as dashed lines in Fig. 2; the x, y, z positions from the calibration are

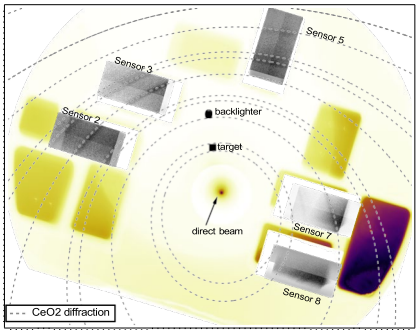

FIG. 2. CeO_2 diffraction collected on Icarus sensors in grey scale, exposed for 2 ns, centered at 24.5 ns. Time integrated image plate is shown in yellow-purple. Dashed grey lines are the calculated CeO_2 diffraction lines using the calibrated BL and sensor positions.

plotted in Fig. 3 and are discussed with respect to the uncertainty in alignment in the next section. The offset in the expected sensor position compared to the calibrated position is used in section V for the compressed lead diffraction.

IV. HOW PRECISE ARE OUR DENSITY MEAUSREMENTS?

We are unable to conduct a location calibration shot for every driven shot using an XRD standard; however, we do have alignment and measurement tools that allow us to estimate the positional uncertainty of the BL, physics package, and sensors. The procedure for target and diagnostic alignment is extensive and covered in detail elsewhere (*11, 12*). Briefly, the Target Alignment System (TAS) is aligned to target chamber center (TCC) using the Chamber Center Reference System (CCRS) prisms which records TCC. The Advanced Tracker Laser Alignment System (ATLAS) then registers TCC using retroreflectors on TAS. The target (physics package and BL) is aligned using TAS; the FIDDLE diagnostic is aligned using 6 retroreflectors on the barrel using ATLAS. Hence, all measurements of position are within the TCC coordinate system.

Uncertainty in the system was estimated from uncertainty in alignment using a Monte Carlo approach with a sample size of 30,000. Using a single pixel on Icarus7, where BCC diffraction has been observed, we report an estimate on our uncertainty in the density measurement from observed XRD peak positions. The multivariate probability density function (*f*) was used to sample x, y, z positions for the BL, physics package, and sensor position (*13, 14*).

$$f = \frac{1}{(2\pi)^{k/2} * \det(S)} * e^{-\frac{1}{2}(x-\mu)^T S^{-1} (x-\mu)}$$

Where the covariance matrix (S) for x, y, z positions:

$$S = \begin{pmatrix} \sigma_{xx}^2 & 0 & 0 \\ 0 & \sigma_{yy}^2 & 0 \\ 0 & 0 & \sigma_{zz}^2 \end{pmatrix}$$

and $\alpha_{BL\ xx,\ yy,\ zz} = 0.3$ mm; $\alpha_{physics\ package\ xx,\ yy,\ zz} = 0.01$ mm; $\alpha_{pixel\ xx} = 0.035$ mm, $\alpha_{pixel\ yy} = 0.025$ mm, $\alpha_{pixel\ zz} = 0.055$ mm, x is a vector defining mean x, y, z positions, and μ is a vector representing a random point with position x, y, z and k is the dimension.

Uncertainties in physics package position was determined by using standard uncertainties assumed by the TAS positioning to be within 10 µm. To generate the sampled positions, we assumed that the entire target volume of the Pb below the pinhole was diffracting; however, given

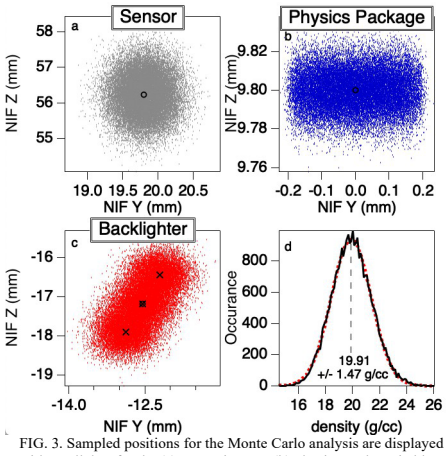

FIG. 3. Sampled positions for the Monte Carlo analysis are displayed with small dots for the (a) sensor in grey, (b) physics package in blue, and (c) BL in red with the center of each BL source marked with an "x". Positions used for the ramp compressed Pb analysis is shown as open circles in (a,b,c). (d) The estimated density distribution given the sampled positions in black from the Monte Carlo sampling; a gaussian fit is shown in the red dotted line.

the X-rays are collimated after they pass through the physics package, we are sampling points that are larger than is physically likely, so the physics package contribution to the measurement's uncertainty is an overestimation.

Prior to positioning in the NIF target chamber, the BL position is metrologized to a location to within a few microns. The uncertainty in BL position was determined to be higher than the physics package given the possibility of the BL behaving much like an arm on the edge of a target that might have some minimal rotation that would lead to a large x,y,z change. We chose a value of 300 µm from a discussion with the TARDIS team from NIF.

Uncertainty for the alignment of FIDDLE incorporates data from three sources. First, we made measurements of the sensor positions and Spherically Mounted Retroreflectors (SMRs) using a Coordinate Measuring Machine (CMM). These five SMRs were mounted slightly vertically offset from the Icarus sensor surface and the sensor/SMR positions were registered with an uncertainty of 5 µm. As the SMR are mounted in front of the sensors, they must be removed for experiments, so the Target Diagnostic Factory (TDF) measured these SMRs and the 6 shot retroreflectors to be used for the shot alignment in the TDF snout frame. Finally, after fieldling FIDDLE six times within the NIF target chamber, we have registered the reproducibility of the insertion as measured with ATLAS.

We estimated the uncertainty in location of the sensor positions in four steps. First, for each experiment, we calculated the rigid body transform from the TDF frame to

the in-chamber measurement of the shot reflectors. Second, this transform was applied to the TDF measurement of the SMR to calculate where they would have been in TCC frame if they had been attached for the experiment. Third, the transform of the SMR locations from the CMM frame to the TCC frame was calculated. Finally, the CMM to TCC transform was applied to the sensors to calculate their positions in TCC frame. From the variability in the sensor placement, the repeatability of the alignment in TCC frame is 30, 20 and 50 μm for x, y, and z, respectively.

For all the BL, physics package, and sensor positions sampled (Fig. 3a,b,c), we calculate the expected 2θ angle—which can be converted into d-spacing and then density for with some knowledge of phase. For BCC Pb, at the observed pixel location, we estimate a density of 19.91 g/cc +/- 1.47 g/cc (1α).

The preliminary calibration values for the BL and sensor positions from the CeO_2 calibration shot (N240402) are reported. The BL position from the calibration is within the sampled positions; ~600 μm from the nominal. The sensor position is ~1.6 mm away from the predicted location. Given the reproducibility of the ATLAS alignment, it is likely we are aligning reproducibly to the same location; however, it is not the nominal location. Hence, our uncertainty reported is more a measurement of our precision, not the accuracy of the diagnostic alignment.

V. RAMP COMPRESSED LEAD DIFFRACTION

The drive and BL pulse shapes have been consistently shaped and timed over 5 NIF shots; representative pulse shapes and interface velocity are shown in Fig 4b and c. By coupling the velocimetry of the Pb/LiF interface, as probed with VISAR with the hydrodynamic simulations from the code HYDRA, the predicted maximum pressure is estimated to be ~110 GPa with approximately an increase of 10 GPa every 1 ns (Fig. 4b).

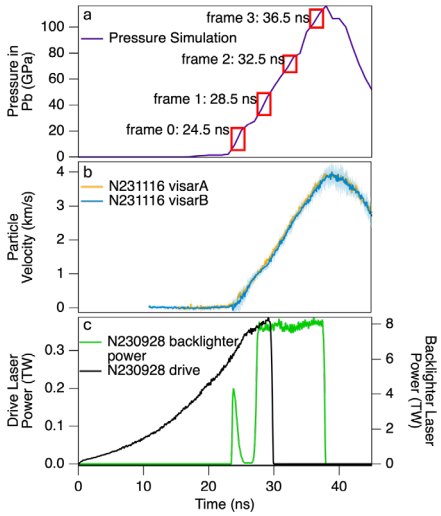

FIG. 4. Temporal history of the experiment showing (a) the pressure, as simulated with hydro codes, with the requested sensor timings in red rectangles, (b) particle velocity, as measured with VISAR, and (c) laser beam pulse shapes to the BL and drive (if used).

Diffraction was collected on ramp compressed lead at three different time (and pressure) steps on sensor 7 on FIDDLE. The raw diffraction patterns were dewarped to a polar view, see Fig. 5a,b,c, so that the diffraction lines appear as vertical lines. The dewarping calculation assumed a point source at the center of the BL and a single source in the target at the center of the diffracting region. Using the offset in sensor position from the expected positions (as calculated from the CeO_2 shot). Red regions in the Fig 5a,b,c are areas that are masked from the integrated lineouts in the bottom of each panel. The regions masked on the low 2θ region of all 3 images are areas of the sensor that are covered with a piece of Ta overreaching the edge of the sensor to protect the master oscillator from being hit with

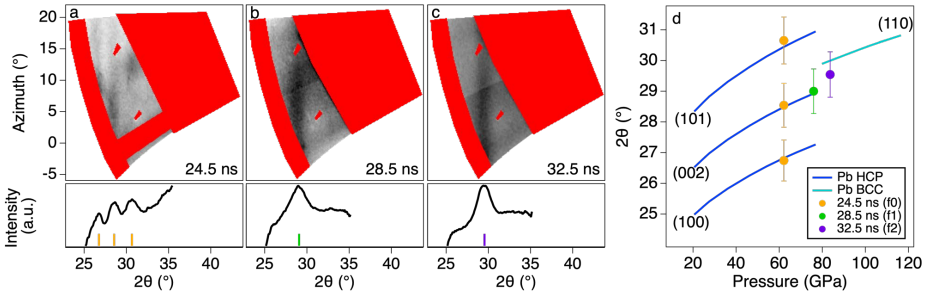

FIG. 5. (a,b,c) Polar view of diffraction. Red regions are masked due to high background. Below each polar image is a lineout, vertically averaged, over the unmasked regions of the image. Tick marks indicate the central peak position for the observed diffraction. (d) Expected 2θ angle plotted against pressure in Pb for HCP and BCC. Observed diffraction peaks are overlain as circles with 1α error bars based on results from section IV.

hot electrons (in early shots, the timing of the sensors was upset by this). In each image, there are small masks that are masking the shadows generated by "sentry" wires that stand out vertically above the sensors and are used to identify the sources of X-ray background. And finally, on the high 2θ region of the images, the background is elevated relative to the region unmasked because it is not shadowed by the target body. An extensive description of the sources of background and mitigation are included in ref. (*15*).

In the first frame, with time centered on 24.5 ns, three peaks are apparent in the diffraction pattern, this is consistent with an HCP structure. The second and third frames, centered at 28.5 ns and 32.5 ns, respectively, contain a single peak, which is consistent with BCC Pb, increases in 2θ between the two frames. This series of three images indicates an increase in pressure between each Icarus frame.

Observed peak positions are overlain on the expected 2θ positions at a given pressure in Fig. 5d. The expected 2θ were calculated from the density from hydrodynamic simulations at a given pressure; for HCP the c/a ratio was assumed to be 1.633. Error bars are based on the uncertainty analysis from section IV. Based on peak positions observed in these 3 frames, the pressure of Pb should be ~60, 80, and 90 GPa. In contrast, hydrodynamic simulations indicate the pressures should be ~20, 40, and 70 GPa at the time we intended to trigger the camera. This disparity in observed pressures may be due to an alignment issue or a timing error (or both). While our sensor timing was tested extensively before installation at NIF, there appears to be a discrepancy in the DIM cabling and timing. In the future, we aim to conduct a dedicated timing calibration shot.

VI. FUTURE WORK

Future work for the FIDDLE diagnostic includes improving the alignment certainty for an improved density measurement. We are actively investigating improving target designs, changing filters in front of the sensors, and improving EMI shielding to decrease the background signal and improve signal to noise. Finally, we will conduct an empirical timing calibration shot in NIF to confirm similar behavior in NIF and the measurements off-line with many repetitions of a short-pulsed laser.

VII. ACKNOWLEDGMENTS

This work performed under the auspices of the U.S. Department of Energy by Lawrence Livermore National Laboratory under Contract DE-AC52-07NA27344.

LLNL-CONF-864496

VIII. AUTHOR DECLARATIONS

A. Conflict of interest statement

The authors have no conflicts to disclose.

B. Author contributions

C. E. Vennari writing, formal analysis, **N. E. Palmer** methodology, **P. R. Nyholm** methodology, **N. Bhandakar** methodology, **S. R. Nagel** supervision, **R. B. Petre** methodology, **C. V. Stan** project administration, **J. H. Eggert** supervision, **D. K. Bradley** supervision, **Y. Ping** funding, **A. Thomas** formal analysis, **D. Swift** formal analysis, **A. C. Carpenter** project administration, **A. J. MacKinnon** supervision, **L. R. Benedetti** conceptualization, formal analysis, writing/reviewing & editing.

IX. DATA AVAILABILITY STATEMENT

Data will be made available with reasonable request.

X. REFERENCES

1. M. A. Barrios *et al.*, Backlighter development at the National Ignition Facility (NIF): Zinc to zirconium. *High Energy Density Physics* **9**, 626-634 (2013).
2. K. Werellapatha *et al.*, Optimized x-ray emission from 10 ns long germanium x-ray sources at the National Ignition Facility. *Rev Sci Instrum* **93**, 123902 (2022).
3. L. Claus, T. England, L. Fang, G. Robertson, M. Sanchez, Douglas Trotter, A. Carpenter, M. Dayton, P. Patel, and J. L. Porter, in *Target Diagnostics Physics and Engineering for Inertial Confinement Fusion VI.* (SPIE, 2017), vol. 10390, pp. 16-26.
4. A. B. L. Claus, T. England, L. Fang, Q. Looker, B. B. Mitchell, A. Montoya, J. L. Porter, M. Sanchez, A. J. Vigil, E. R. Hurd, A. Carpenter, M. Dayton, C. E. Durand, G. Rochau, in *Radiation Detectors in Medicine, Industry, and National Security XIX*. (SPIE, 2018), vol. 10763, pp. 135-146.
5. K. Werellapatha *et al.*, Time-resolved X-ray diffraction diagnostic development for the National Ignition Facility. *Rev Sci Instrum* **95**, (2024).
6. J. R. Rygg *et al.*, X-ray diffraction at the National Ignition Facility. *Rev Sci Instrum* **91**, 043902 (2020).
7. A. Dewaele, M. Mezouar, N. Guignot, P. Loubeyre, Melting of lead under high pressure studied using second-scale time-resolved x-ray diffraction. *Physical Review B* **76**, (2007).
8. N. Palmer, *Review of Scientific Instruments*, (submitted; this collection).
9. L. R. Benedetti *et al.*, Timing characterization of fast hCMOS sensors. *Rev Sci Instrum* **92**, 044708 (2021).
10. P. Nyholm, *Review of Scientific Instruments*, (submitted; this collection).
11. N. D. Shingleton, NIF Target Alignment System, TAS 2. (2019).
12. G. Brunton, Abed, Y., Fedorov, M., Fishler, B., Larson, D., Ludwigsen, A.P., Mathisen, D., Miller-Kamm, V., Paul, M., Reed, R. and Speck, D., in *Proceedings of the 16th Int Conf on Accelerator and Large Experimental Control Systems (ICALEPCS)*. (Barcelona, Spain, 2017), pp. 8-13.
13. R. O. Duda, P. E. Hart, D. G. Stork, *Pattern Classification*. (Wiley, New York, ed. 2, 2001).
14. A. Papoulis, *Probability, Random Variables, and Stochastic Processes*. (Wiley, New York, ed. 3, 1991).
15. L. R. Benedetti, *Review of Scientific Instruments*, (submitted; this collection).